PCCP

Deprotonation of Phenol linked to a silicon dioxide surface using Adaptive Feedback Laser Control with a Heterodyne Detected Sum Frequency Generation Signal

Journal:	*Physical Chemistry Chemical Physics*
Manuscript ID	CP-ART-12-2021-005613.R2
Article Type:	Paper
Date Submitted by the Author:	15-Jun-2022
Complete List of Authors:	Goun, Alexei; Princeton University, Chemistry Frederick, Esther; Princeton University, Chemistry; Sandia National Laboratories Er, Ali; Princeton University, Chemistry Bernasek, Steven; Princeton University, Chemistry; Yale-NUS College, Science Rabitz, Herschel; Princeton University, Department of Chemistry

Deprotonation of Phenol linked to a silicon dioxide surface using Adaptive Feedback Laser Control with a Heterodyne Detected Sum Frequency Generation Signal

Alexei Goun[1], Esther Frederick[2], Ali O Er[1], Steven L. Bernasek[3], Herschel Rabitz[1]

[1]Department of Chemistry, Princeton University.

[2]Sandia National Laboratory, Albuquerque, New Mexico,

[3]Division of Science, Yale-NUS College, Singapore

Abstract

The development of laser-controlled surface reactions has been limited by the lack of decisive methods for detecting evolving changes in surface chemistry. In this work, we demonstrate successful laser control of a surface reaction by combining the adaptive feedback control (AFC) technique with surface sensitive spectroscopy to determine the optimally shaped laser pulse. Specifically, we demonstrate laser induced deprotonation of the hydroxyl group of phenol bound to a silicon dioxide substrate. The experiment utilized AFC with heterodyne detected vibrational sum frequency generation (HD-VSFG) as the surface sensitive feedback signal. The versatile combination of AFC with HD-VSFG provides a route to potentially control a wide range of surface reactions.

I. Background

Lasers hold great promise as a tool for manipulating chemical reactions due to their ability to precisely control transformations of molecules. In such circumstances, laser irradiation of molecules can lead to highly complex molecular processes requiring careful shaping of the laser pulse to direct the reaction along the desired pathways. The optimal laser pulse features are typically difficult to reliably design, often due to the lack of full knowledge of the system Hamiltonian and the complexity of the necessary calculations. Adaptive feedback control (AFC),

sometimes referred as a learning control, can sidestep these difficulties by directly operating in the laboratory[1-3] to provide an effective and efficient technique for determining the optimal pulse features to meet the desired goal. The procedure has been applied to wide ranging scenarios from controlling gas-phase reactions[4, 5] out to manipulating complex biomolecules in solution[6, 7] .

Advanced manufacturing, such as nanoscale integrated technologies and complex detection systems, often rely on increasingly elaborate surface features that, in turn, require precise control of surface reactions[8-11]. In an attempt to meet the latter needs, traditional surface chemistry (e.g., by means of electrochemistry and *linearly* photo-driven chemical reactions) often cannot selectively produce the desired surface species, while also resulting in a multitude of unwanted products. Thus, tailored optical control of surface reactions has become an increasingly important goal. In this work, we develop an AFC technique for control of surface reactions by using feedback from heterodyne detected vibrational sum frequency generation (HD-VSFG) to determine the shape of the laser pulse needed to guide a targeted surface bound molecule along a particular reaction pathway. As an illustration, we demonstrate AFC combined with HD-VSFG for deprotonation of the hydroxyl group of phenol surface-bound to a silicon dioxide substrate.

The use of lasers to initiate a particular chemical reaction has a variety of advantages, such as spatial accuracy and the ability to rapidly execute the process. A variety of laser-based approaches have been developed to control reactions, including multiphoton excitation through the phase structure of the excitation beam,[12] modification of the intramolecular potential through AC Stark shift effects,[13] and rapid adiabatic passage.[14] Ultrafast laser pulse shape control, in particular, possesses several unique properties that enable selective and precise molecular manipulation. Due to the short pulse duration of less than a picosecond, ultrafast lasers can routinely achieve the high field strengths (i.e., comparable to intramolecular interactions) needed

to manipulate reactions, potentially leading to products beyond the capability of traditional chemical kinetics. The latter circumstances can be facilitated by the light-matter stimulated reaction being of a highly non-thermal nature. In this fashion, the duration of the *optimally shaped* laser pulse also can be of the same order of magnitude or shorter than the molecular motion, thereby allowing the laser energy to access only the relevant degrees of freedom. The temperature rise of the surface can be made negligible under appropriate conditions, which can preserve the integrity of the sample while accomplishing the desired laser action. Combining these features, in principle, opens up the freedom for appropriate optical pulses to direct the molecular dynamics towards desirable reaction pathways.[1, 4, 15-17]

As further background with regard to the demonstration presented in the paper, coherent control of surface reactions has remained an open challenge for many reasons. A prime issue has been the lack of a surface species selective feedback technique possessing a high-fidelity signal that can be recorded at the rapid pace needed to effectively monitor the evolving reaction yield as the laser pulse shape is guided by AFC. As far as we know, only one experiment has been published demonstrating optical control of surface reactions,[18, 19] but this experiment indirectly monitored the surface reaction through mass spectroscopy of gas phase products dissociated from the surface. The lack of a direct surface monitoring method is a drawback, because a particular gas phase specie is not guaranteed to unequivocally result from a surface reaction, as additional gas phase dissociative dynamics may occur. Furthermore, only ionic species may be observed using mass-spectroscopy, and the technique is limited to high vacuum conditions, preventing applications under common ambient experimental circumstances in surface chemistry.

In this paper, the previous challenges are overcome by introducing an AFC method, which guides the optimization by a direct high quality, surface specific feedback signal from HD-VSFG.

Importantly, HD-VSFG is a universal technique for providing a feedback signal for the progress of laser-controlled surface reactions by utilizing vibrational sum frequency generation (SFG), which is tailored for selectively analyzing surface processes[20, 21]. SFG relies on irradiating a surface with two input pulses, one being a broad infrared (IR) bandwidth and the other consisting of a narrow visible or near infrared pulse. The spectrally broad IR pulse vibrationally excites the species on the surface of the sample. The spectrally narrow pulse induces a Raman process by interacting with the vibrationally excited species, thus resulting in a spectral shift characteristic of the surface species. Due to symmetry restrictions, SFG is strictly prohibited within the bulk of centrosymmetric materials [22, 23]. As the surface breaks the material symmetry, the resulting output beam will contain information specific to the surface. However, the use of SFG for probing optical surface reactions has been limited due to the weak signal resulting from both the inherently small number of surface species and the natural low signal strength of the Raman effect. Both of these limitations were recently overcome with the introduction of heterodyne detection,[24,25] which amplifies the SFG signal by coherently combining it with an additional beam. Heterodyne detection can also provide information about (monolayer) orientation, allowing for characterization of surface morphology[24].

The present paper will demonstrate AFC of O-H bond breaking from a surface-bound phosphonated phenol self-assembled monolayer (SAM), schematically shown in Figure **1**.

Figure 1: Schematic representation of phosphonated phenol molecules bound to a silicon dioxide surface where the hydroxyl group undergoes optically induced deprotonation.

There are several reasons we chose surface-bound phenol as a convenient system to demonstrate a laser driven reactive transformation. One factor is that the control pulse centered at 400nm wavelength draws upon the electronic properties of phenol to allow for two-photon induced deprotonation. Concomitantly, it is impossible for the control or the SFG detection pulses to linearly contribute to the photochemical process, and this circumstance avoids the masking of the non-linear, coherent two photon 400nm control contribution (see Figure **2**). In particular, the electronically excited state of the phenol is at ~5eV, so it is impossible for it to be activated by linear excitation with the Raman laser pulse at the frequency of 795nm or its second harmonic used as a control beam at 400nm. The strongest optical transition of the phenol corresponds to $\pi \rightarrow \pi^*$ at 260nm. The π^* state forms a conical intersection with the σ^* dissociative state[26-28]. At large separation of the proton from its parent molecule, σ^* becomes the ground state. As the reaction is exoergic, the phenol can be deprotonated even in the vacuum[28] and does not require additional stabilization by polar solvent molecules, typical for other deprotonation reactions. The relevant energy states, together with optical transition energies are illustrated in Figure **2**. Thus, the surface bound phenol deprotonation reaction serves as a good example since it utilizes a reliable, easily observable surface species transformation resulting from exploiting the manipulation of the O-H vibrational wavepacket combined with level crossing dynamics. As the phenol negatively charged ion and proton are under Coulomb attraction, there is expected to be a tendency for the recombination reaction, typically taking place on a nanosecond to microsecond time scale[29]. Thus, between reactions of light induced phenol deprotonation and recombination, there is an ample temporal window when the efficiency of an optical excitation to remove the proton can be quantified over a time period of 100 picoseconds after the arrival of the control pulse. In the proposed experiment during a later time window, the remaining amount of the sample attached

surface O-H group is measured. A fresh surface sample was used for each control experiment and given the focus of the experiment on bond breaking no attempt was made to follow a subsequent reprotonation. Besides the phenol groups, water molecules are likely attached to the sample surface as it is exposed to the laboratory environment. At the same time, the potential additional process of photoinduced water decomposition should not play a prominent role as it occurs at a wavelength shorter than 200nm and is not expected to affect the O-H bond of the phenol.

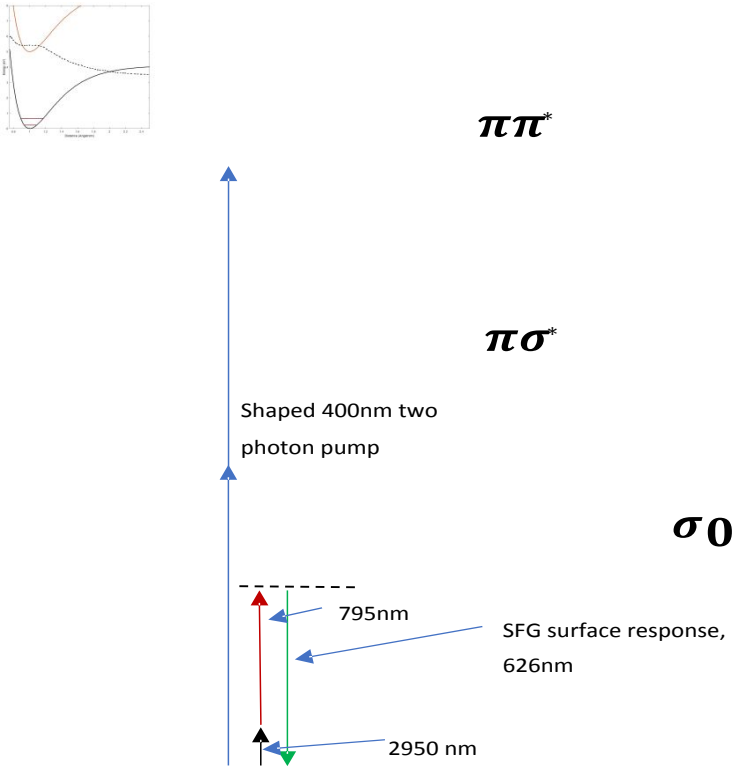

Figure 2. Energy diagram of the combined phenol photodissociation reaction and SFG composition detection. The length of the arrows and energy levels are drawn to scale. The colors of the photonic arrows are chosen for graphical clarity. The detection of the O-H group *presence* is carried out with SFG utilizing the vibrational manifold of the ground electronic state, indicated in the lower portion of the figure. The excited, dissociative product can be optimally achieved by two photon absorption of a 400nm, suitably shaped, laser control pulse.

II. Experimental Methods

A. Surface sample preparation.

This section describes the procedure to create the particular SAM used in the subsequent laser control experiments. A hydroxy terminated SAM was formed by deposition of 4-hydroxybenzylphosphonic acid onto a SiO_2 substrate wafer 1cm x 1cm in size, via a well-known tethering by aggregation and growth (T-BAG) procedure[30]. The SiO_2 wafers were vertically suspended in a solution of ~47 μM 4-hydroxybenzylphosphonic acid (≥95% purity, Sigma-Aldrich) in THF. As the THF evaporates, what remains is a well-ordered SAM physisorbed on the SiO_2 through hydrogen bonds between the phosphonic acid and SiO_2. The silicon wafer was then heated for ~12 hours to convert the physisorbed phosphonic acid SAM to a chemisorbed phosphonate-SiO_2 monolayer. This process was repeated three times with the same wafer to obtain a good quality monolayer with high molecular packing density.

Surface characterization was carried out by several means. The SAM formation and uniformity was confirmed using ellipsometry, contact angle goniometry and atomic force microscopy (AFM). X-ray photoelectron spectroscopy (XPS) and ATR-FTIR were used to determine the composition of the monolayer. These processes are described further below.

Stokes Ellipsometry measurements were made (Gaertner Scientific Corp., USA) using a helium-neon laser (633 nm) source at a fixed incident angle of 70°. The refractive index of silicon and the organic layer was chosen to be 3.85 and 1.5, respectively. A number of points across the sample were measured, which assured uniformity. The contact angle goniometry data was collected under ambient conditions. A drop of Millipore water (~2 μL) was placed on the sample

surface to form a sessile drop from which the contact angle was measured by a Theta Optical Tensiometer (KSV Instruments, Finland). The ellipsometry determined thickness was 23 ± 1 nm and the contact angle was 32 ± 2 deg. This result confirms the formation of a reasonably uniform hydrophobic SAM relative to the native oxide contact angle of near zero deg.

The XPS measurements were performed using a Mg Kα X-ray source (1253.6 eV) and an electron spectrometer (VG ESCALAB MkII) operated in constant analyzer energy mode with a pass energy of 100 eV and 20 eV for survey and high-resolution scans, respectively. The data was analyzed using CasaXPS software. A linear baseline was used for s peaks (O(1s), C(1s)), while a Shirley baseline was used for p peaks (P(2p), S(2p), Si(2p)). All peaks were calibrated to adventitious carbon at 284.8 eV and fit using a Gaussian-Lorentzian peak shape.

Analysis of the C(1s), O(1s) and P(2p) XPS spectra (Figure 3) indicate the successful deposition of the molecules through the formation of a phosphonate bond. XPS of the C(1s) displayed three discernable peaks at 284.8 eV, 285.8 eV and 289.2 eV with a fitting residual of 1.0 on the scale in Figure **3**. The 284.8 eV peak was attributed to adventitious carbon while the peak at 285.8 eV was attributed to the C-O and C-P carbons, corresponding to C(1s) literature phenol values of 284.5 eV - 286.1 eV for C-O,[31] and C-P values of 286 - 286.4 eV [32]. Differentiation of individual C(1s) peaks was problematic with measurements of this resolution. The weak 289.2 eV peak was characteristic of values typically seen for carboxylic acid, which indicates the likely presence of adsorbed COOH species. The P(2p) region displayed a broad peak at 132.1 eV fit with a residual of 1.1. This peak corresponds well to P(2p) binding energies for molecules containing PO_3, which range from 132. 7 - 134.7 eV depending on the chemical environment; due to overlap with the Si 2p plasmon, the peak cannot be definitely assigned to PO_3 [33]. The O(1s) spectrum displayed a weak peak at 532.6 eV. The peak fit implied the presence of more than one oxygen

species but the data was not of high enough resolution to de-convolute reliably. The peak was attributed to both adventitious oxygen between 532 - 533 eV and hydroxyl, for which the published value from C_6H_5OH is 531.7 eV [34]. ATR-FTIR was carried out to confirm the presence of a hydroxy group, as explained below.

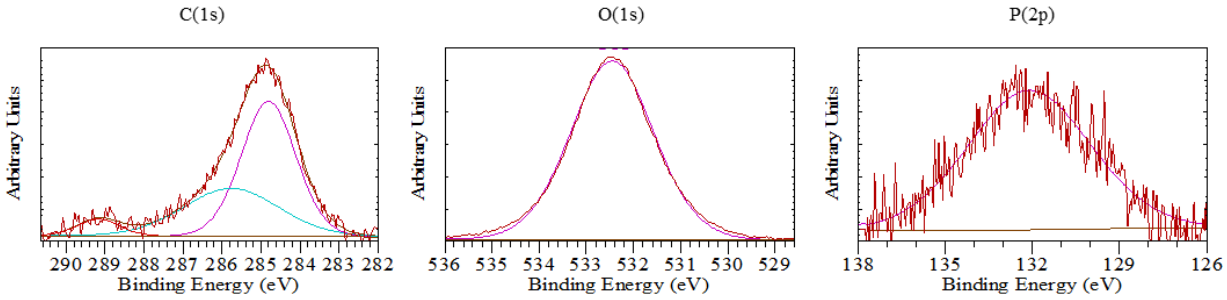

Figure 3: XPS of the 4-hydroxybenzylphosphonate SAM C(1s), O(1s) and P(2p) regions (see the text for details). The broad O(1s) signal could not be deconvoluted into the adventitious and hydroxy group components, so ATR-FTIR (Figure 4) was carried out to confirm the presence of a hydroxy terminating species.

The ATR-FTIR measurements were made under ambient conditions using a Nicolet 6700 FT-IR spectrometer with a diamond ATR-FTIR accessory (Thermo Electron Corp., USA). The accessory crystal of the ATR-FTIR was cleaned with isopropyl alcohol before the background reference was collected. Scans were manually corrected via a linear baseline, then ATR corrected and smoothed. All spectra were taken with clean SiO_2 as a background reference, which was automatically subtracted from the spectra. Therefore, the observed peaks are assumed to be characteristic of the SAM. The ATR-FTIR spectra (Figure **4**) displays a broad peak running from 2700 to 3500 cm^{-1} which was attributed to the hydroxyl stretch vibration consistent with values of 2600 – 3300 cm^{-1} from solution and vapor phase IR spectra[35]. In summary, the combination of the XPS and ATR-FTIR data confirmed the chemisorption of hydroxyl terminated molecules bound through a phosphonate bond to the SiO_2 surface.

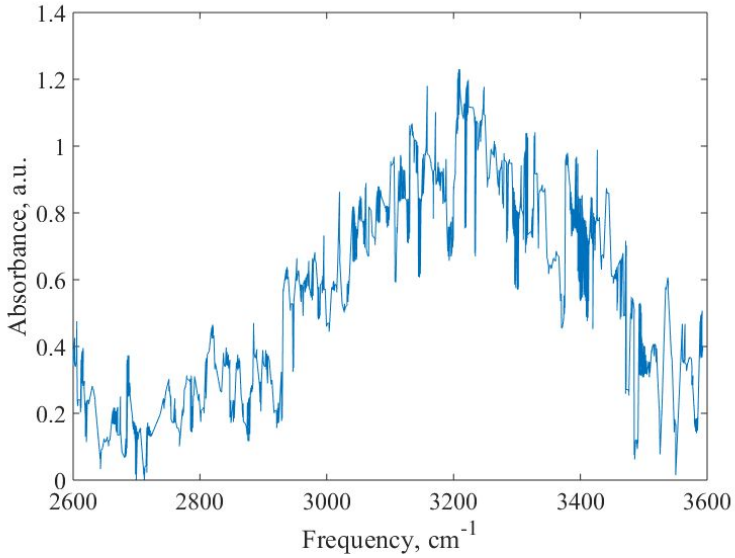

Figure 4: ATR-FTIR of the 4-hydroxybenzylphosphonate SAM displayed a broad peak stretching from 2700 ~ 3500 cm^{-1} corresponding to hydroxyl vibration, which confirms the presence of a hydroxy terminating group.

B. Laser control apparatus.

A Coherent Legend Ti:Sapphire regeneratively amplified ultrafast laser system with a repetition rate of 1 kHz and pulse length of ~40 fs was used to generate 800 nm laser pulses, which were then split in two equal parts. One part (i.e., upon doubling to 400nm) formed the basis for control of O-H bond breaking and the other part was utilized with an Optical Parametric Amplifier (OPA) to form two pulses to monitor the surface with HD-SFG (Figure **5**). The role of the latter two pulses at 795nm and 2950nm for generating the SFG signal at 626nm is shown in Figure **2**. The 800nm beam was frequency doubled to 400 nm with a 50 micron thick BBO crystal and the temporal shape of the latter laser pulse was modulated as the control using a standard ultraviolet pulse shaper.[36] Upon entering the pulse shaper the beam was first spectrally dispersed by a grating with 2400 lines/mm in Littrow configuration. Each spectral component was focused into a wide aperture acousto-optic modulator crystal with a spherical mirror of 50cm focal length. The phase

and amplitude of an acoustic beam could both be modulated by a computer-driven arbitrary waveform generator. When the optical control pulse diffracts from an acoustic grating, the predetermined pattern of the amplitude and phase is imprinted onto the spectral components of control pulse centered at the 400nm beam. Thus, the action of the pulse shaper in the frequency domain can be described as

$$E_{out}(\omega_j) = A(\omega_j)exp(i\varphi(\omega_j))E_{in}(\omega_j) \quad (1)$$

where $E_{in}(\omega_j)$ is the input spectrum of the optical pulse centered at 400nm and having 20nm full width at half maximum, $A(\omega_j)$ is the amplitude of the acoustic wave at the location in the crystal corresponding to the spectral component ω_j, $\varphi(\omega_j)$ is the associated phase of the acoustic wave, and $E_{out}(\omega_j)$ is the optical field after the interaction with the shaped acoustic waveform imprinted in the crystal. Before exiting the pulse shaper, the spectral components were recombined into a collimated, temporally shaped control pulse by a second grating and spherical mirror.[36] The latter temporally shaped control pulse was focused perpendicular to the surface of the sample using a combination of 20cm focal distance lenses and mirrors. In all of our experiments the amplitude $A(\omega_j)$ parameters were not varied, and the pulse shaping variation for control purposes was confined to the phase $\varphi(\omega_j)$; in this fashion, the shape of the control laser pulse was varied while the pulse energy was kept constant. This procedure suppresses the potential influence of thermal effects at the surface due to a temperature rise, albeit small, which will be the same for all pulses used in the experiment as it is not expected to be dependent on the temporal intensity of the pulse, rather only on its energy content. The surface thermal effects will be discussed later in the paper.

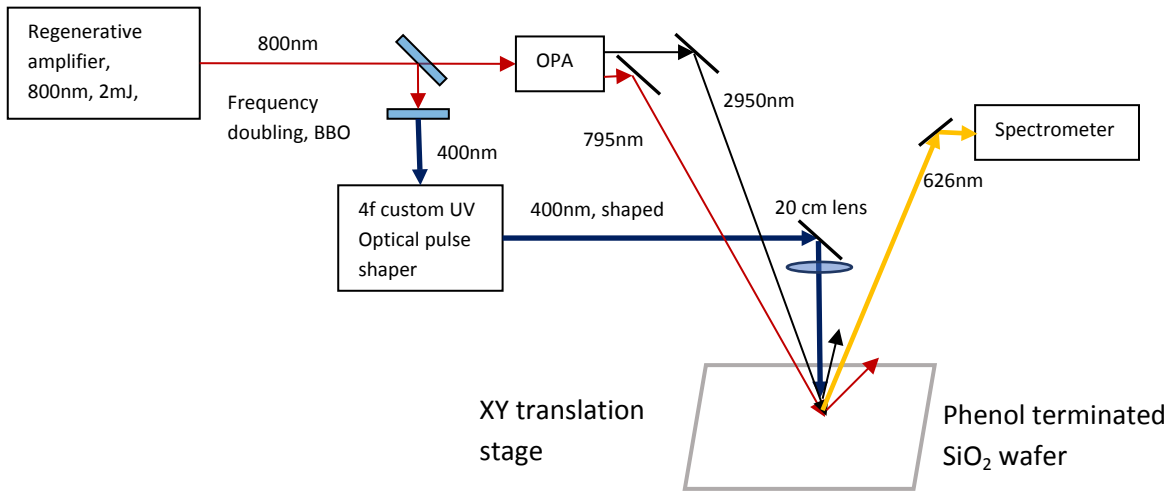

Figure 5. Control and detection apparatus setup (simplified to show general features): A primary 800 nm pulse from the laser was split into two parts – one 800nm pulse beam was frequency doubled to 400nm and modulated with the acousto-optic pulse shaper for phase variation to form the control pulse. The second 800nm pulse beam passed through an optical parametric amplifier (OPA) to generate the HD-SFG infrared beams (i.e., at 795nm and 2950nm red and black, respectively, in the figure) used to monitor the surface reaction. The resulting three beams were then focused onto the surface using a series of mirrors, simplified in this schematic by a single mirror for each beam. The resulting SFG beam at 626nm (orange) was collected by using a series of mirrors to send it to the spectrometer; further details of the SFG process are shown in Figure 6. The experiment was carried out at ambient laboratory conditions, with the SAM sample described earlier.

The second part of the initial 800nm pulse beam was further split upon entering the OPA to be used for HD-SFG spectroscopy to monitor the change in surface chemistry, as mentioned earlier. A broad bandwidth mid-IR pulse beam was generated by the OPA with a central wavelength of 2950 nm and an energy of 5 μJ (see Figure **5**), which was focused on the sample using a CaF_2 lens with an 8cm focal length. Simultaneously, the 800nm pulse beam was spectrally narrowed by an interference filter into a beam centered at 795nm with a bandwidth of 1nm, which was focused on the surface with a 20cm focal length fused silica lens. The control and the two detection beams were overlapped using a 50 micron diameter pinhole to ensure good spatial overlap at the surface. The pulse beams impinging on the sample surface resulted in two reflected beams centered at 795nm and 2950nm and produced a third SFG beam centered at 626nm, which

contained the surface composition information. The bandwidth of 795nm pulse is 1nm that corresponds 15cm^{-1}, limiting the spectral resolution to ~30cm^{-1}. This resolution is efficient for detecting O-H but does not permit resolving the C-H stretch in the recorded spectrum[37].

The two SFG excitation pulses (centered at 795nm and 2950nm) reflected from the surface of the wafer were later utilized (see Figure **6**) for heterodyne pulse generation, while the 400nm shaped control pulse normal to the surface retroreflected and was not further collected.

The SFG signal was strengthened using Yamaguchi's heterodyne amplification approach[24]. The geometry of HD-SFG is illustrated in Figure **6**; the beam color scheme is consistent with Figure **5**. In brief, the resulting SFG pulse beam spatially separates from the other reflected beams and is transmitted through a 1.2mm thick glass slide to optically delay each pulse by 2.1ps. All three beams were then reflected by a spherical mirror with a 5cm radius of curvature to cross again on a non-centrosymmetric GaAs surface; in this fashion, the 2950nm and 795nm pulse beams generated a second SFG signal that traveled along the same path as the original SFG pulse beam with both beams spatially and temporally overlapping. The temporal overlap of the signal and heterodyne pulses occurs in the spectrometer. The SFG beam generated from GaAs resulted in a strong Local Oscillator (LO), which creates a spectral interference pattern on the surface of the CCD detector. In such a configuration, the spectrally resolved signal on the CCD array, $I(\omega)$, can be represented as

$$I(\omega) = |E_{LO}(\omega) + exp(i\omega\tau)E_S(\omega)|^2 = |E_{LO}(\omega)|^2 + 2Re\big(exp(i\omega\tau)E_{LO}^*(\omega)E_S(\omega)\big) \quad (2)$$

where $E_{LO}(\omega)$ is the electric field of the LO, $E_S(\omega)$ is the SFG electric field signal from the surface sample under control, τ is the 2.1 ps time delay between the signal and the LO, and ω is the optical frequency at 630nm.

In order to recover the spectrum of the surface we have relied on a well know property of the Fourier transform that the spectrum of the pulse shifted in the time domain is the original spectrum with additional phase modulation $FT(f(t-\tau)) = FT(f(t))exp(i\omega\tau)$. Thus, to identify the spectrum of the pulse generated by SFG, the side peak (i.e., either of the side peaks in Figure 7b later) of the Fourier transform was shifted to the origin and the inverse Fourier transformation was performed [37, 38] (see Figure **7c** later).

The field generated by the sample's surface might also contain the contribution of higher order processes such as $\chi^{(3)}$, especially in the presence of strong electrostatic fields due to charge separation on the surface [39]. This additional contribution can influence the exact shape of the SFG spectra but does not change its correlation to the protonation degree of the phenol's hydroxyl group. The second term on the RHS of Eq. (2) provides amplification along with the presence of frequency modulation $exp(i\omega\tau)$ of the weak surface signal. The surface signal comes as a product with local oscillator in the spectral domain, separating these contribution requires additional calibration experiment[37]. Both the real and imaginary part are both linearly proportional to the amount of hydroxyl radicals at the surface. Even though the spectral shape might be perturbed by the interference between the real and imaginary part, the magnitude of the signal is still proportional to the amount of O-H on the surface. The response of the surface includes contributions from all of the constituents of the surface, their resonant and non-resonant contributions. Due to the long delay of 100 picoseconds between the control and the probe pulses all of the coherent processes are over, and the nonresonant contributions should remain the same from pulse-to-pulse. The only components of the surface that actively interacts with the control pulse are the phenols groups

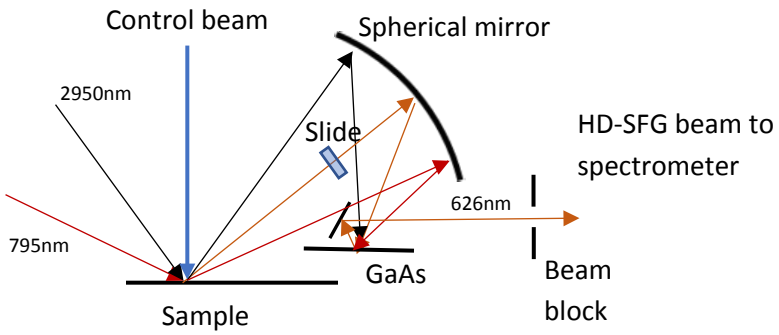

Figure 6. The sample with sum frequency and local oscillator sum generation geometry. See the text for details.

To obtain the surface sensitive information, a spectrum was acquired using an Andor Shamrock 300 spectrometer equipped with an Andor Newton EMCCD camera. The surface vibrational spectrum of the sample was isolated from the two combined SFG beams with Fourier transformation filtering. The SFG signal recorded by the CCD (Figure **7a**) displayed high frequency modulation due to the interference between the GaAs generated heterodyne LO and the surface generated signal. The high-frequency spectral modulation corresponds to the 2.1ps optical delay. Once the optical spectrum is Fourier transformed, the signal shows clear peaks at ~±2.1ps. The spectroscopic peak at 2.1ps was subsequently down shifted to be centered at zero-frequency. A second inverse Fourier transformation displays the desired spectrum of the surface monolayer, with an extremely broad peak from 2700 – 3700cm^{-1} attributed to the O-H group in the phenol (Figure **7c**). Importantly, the identified spectrum in Figure **7c** shows overall consistency with the phenol spectra of Figure **4**, measured by transmission spectroscopy.

III. Optimization of O-H bond breaking.

The integrated intensity of the surface bound O-H vibrational spectrum in Figure **7c** served as the AFC signal for laser pulse shape optimization to enhance breaking the phenol O-H hydrogen-oxygen bond. The delay between the control pulse and the HD-SFG pulses was set at 100 picoseconds[40]. An advantage of using a monolayer with phenol as the exclusive photoactive

species is that only the total peak area in Figure **7c** is needed for the surface composition feedback optimization signal. By utilizing a broadband femtosecond laser, the technique provides an instantaneous probe of more than ~1000cm^{-1} of bandwidth, as evident in Figure **7c**. A period of 10 seconds of signal averaging was sufficient to obtain reliable data (9 seconds of data collection and 1 second delay between consecutive control pulse shapes). The surface was placed on a translation stage such that each control laser pulse combined with its interrogating response was applied at a new location on the sample for signal averaging. The translation speed of the sample was 30 microns per second. The sample was raster scanned in X and Y directions. The spacing between successive horizontal scans was 100 microns.

A standard genetic algorithm was used to guide the optimization of the AFC experiment. The algorithm consisted of a 30 member population of pulses per generation[41]. Each generation was placed on a separate scan line of the sample. The sample was 1x1 cm in size, which allowed a space for ~90 generations of the optimization. At each optimization step the mutation rate was 10% and the crossover rate was 25%. As stated earlier, the shaped optical control pulse centered at 400nm was chosen such that it has no linear absorptive bond-breaking interaction with the surface bound molecular sample. The control pulse was compressed to ~ 50fs duration in free space. The control beam interacts with the molecules at second order for deprotonation, which is physically significant; if a linear first order interaction with the field is present, then it would likely dominate the optical response and lose the physical significance of the control phase modulation. In contrast, the second order interaction is sensitive to the shape of the electromagnetic field, which is captured by the spectrum being second order in the electric field, $E^{(2w)}(\omega)$,

$$E^{(2w)}(\omega) = \int E(\omega_1)E(\omega - \omega_1)d\omega_1 \quad (3)$$

where $E(\omega_1)$ is the shaped electromagnetic field centered around 400nm. Consequently, the efficiency of the two-photon excitation is proportional to the spectral overlap of the complex

surface bound molecular susceptibility $\alpha(\omega)$ spectrum with $E^{(2w)}(\omega)$. In terms of the control amplitude $A(\omega)$, control phase $\varphi(\omega)$, and the initial optical field $E_{in}(\omega)$ of equation (1), the two-photon excitation probability becomes

$$P_{ex} = \iint \alpha(\omega)\exp(i(\varphi(\omega_1) + \varphi(\omega - \omega_1)))A(\omega_1)A(\omega - \omega_1)E_{in}(\omega_1)E_{in}(\omega - \omega_1)d\omega d\omega_1 \quad (4)$$

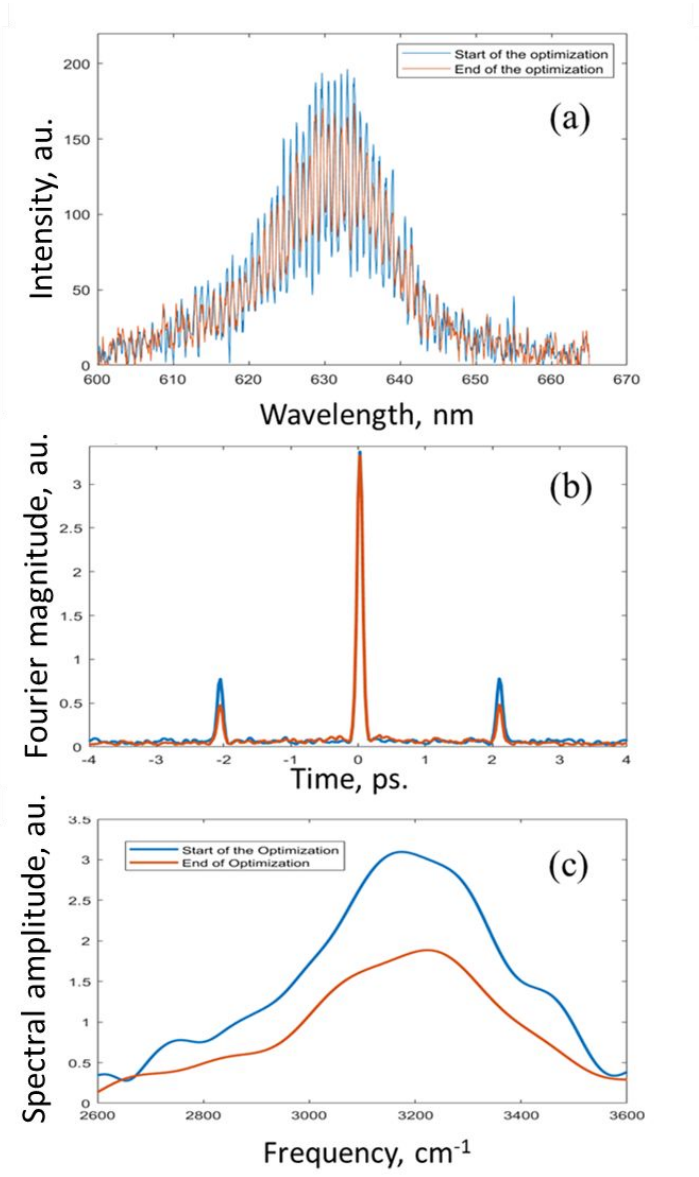

Figure 7 (a) Spectral interference recorded by the CCD. Here, and in (b) and (c), the blue color corresponds to the start of the optimization, and the red color refers to the results at the end of the optimization. (b) Fourier transformation of the intensity distribution in (a). (c) Vibrational spectrum of the surface sample (see the text for further details), which is attributed to the O-H stretch consistent with that shown in Figure **4** by direct surface absorption over the large sample area. The reduction in the OH signal from the initial and final pulse corresponds to the results shown in Figure **8a**.

The efficiency of the two-photon absorption and subsequent deprotonation can be manipulated by the presence of phase factor $\exp(i(\varphi(\omega_1) + \varphi(\omega - \omega_1)))$, which can be varied to maximize P_{ex}.

The successful use of the SFG feedback signal in the AFC experiments to enhance the breaking of the O-H bond was demonstrated utilizing a genetic algorithm to guide the evolving sequence of control fields. An initial transform limited field was utilized (i.e., included in the population of the 1st genetic algorithm generation) coming from the pulse shaper as determined by optimized self-diffraction in a quartz crystal. The genetic algorithm optimization identified a shaped pulse with a ~40% decrease in the O-H bond signal after only ~90 generations. The most effective laser pulse at the last generation was produced by a phase mask with a complex form (i.e., digitized over equally spaced spectral windows) shown in Figure **8b**. The optimized temporal pulse intensity in Figure **8c** was obtained by the Fourier transformation of the phase mask. A full interpretation of the control mechanism is likely complex, as implied by the temporal intensity profile in Figure **8c,** possibly including coupling to the electrons in the phenol benzene ring, and the details of the conical intersection crossing in Figure **2** that eventually lead to the loss of the hydrogen. Furthermore, the continuing decrease in the deprotonation signal in Figure **8a** suggests that further AFC optimization could lead to a higher yield. The broad spectrum of the O-H stretch likely implies the expected presence of water on the surface of the sample. The two-photon absorption of water occurs in the wavelength range shorter than 200 nm and is not accessible for the second order process driven by 400nm pulse. Future investigation will be needed to clarify the role of the surface water in the coherent control of phenol in the deprotonation process. Finally, we remark that the pulse shape on the surface of the sample might be significantly different from that of the pulse in free space. The surface molecules are illuminated by the incident and surface reflected waves possibly along with the complex optical interactions. Only further, likely

elaborate, experiments could reveal the underlying details of the OH bond breaking control mechanism.

Utilizing ultrafast optical pulses for promotion of a chemical reaction can render thermal effects as negligible. This matter is particularly important with surface chemistry where heating could interfere with the shaped control field dynamical effects. The SAM is functionalized with a thin layer of SiO_2 that is transparent to 400nm radiation. For the temperature rise estimate we take a worst-case scenario of considering the underlying substrate to be strongly absorbing Silicon. As an assessment of this issue, the refractive index of bulk silicon at 400nm is 5.56, consequently the reflection coefficient of silicon is 0.48. Therefore, for a single laser pulse only ~ 0.52 microjoule is transmitted into the silicon bulk. For a 100 micron beam waist, typical upon application of the 400nm laser pulse in our experiment, we estimate that the temperature rise on the surface is limited to ~95°C. The phenol O-H bond dissociation enthalpy obtained by photofragment dissociation spectroscopy[42] is 364.7kJ/mol. The thermal energy k_BT after pulse absorption, assuming a temperature rise of 95°C, is 3.27kJ/mol. Thus, the thermal energy is two orders of magnitude smaller than the dissociation energy of the O-H bond, consequently the effect of the temperature rise is expected to be negligible in the present experiments. The Si-O bond has an even higher dissociation energy of 452 kJ/mol and should stay intact. The same conclusion can be reached for all other covalent bonds involved in the experiment.

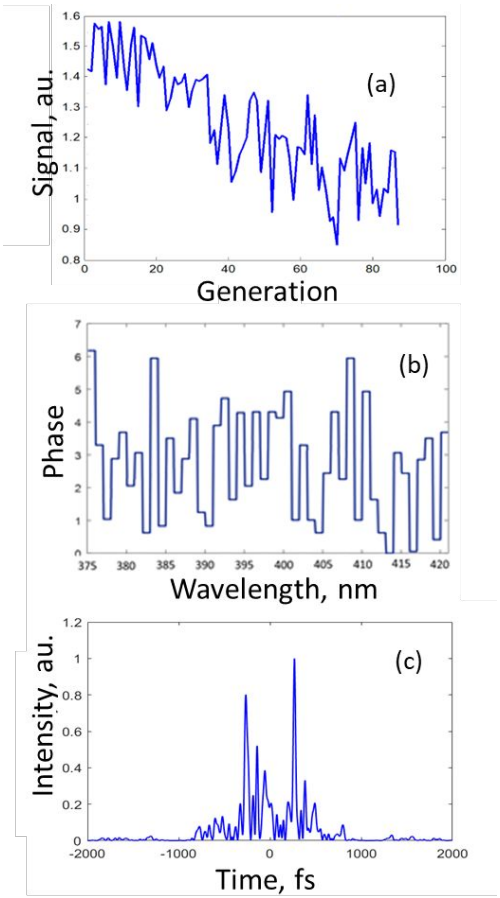

Figure 8. Quantum control optimization of deprotonation from the phenyl O-H bound to the surface sample (see Figure **1**). (a) The genetic algorithm optimization identified a shaped pulse that is 40% more effective at desorption (Generation 88) than an unshaped laser pulse (Generation 1); the output of the best pulse that results is shown in each generation. (b) The digitized acousto-optic phase mask, corresponds to the final best pulse in (a) at generation 88. (c) Temporal pulse intensity of the field corresponding to the mask in (b) The evident structure implies that complex dynamics are likely occurring to produce the deprotonation process.

III. Conclusion.

In summary, we have experimentally demonstrated the ability to control a specific surface reaction (i.e., O-H deprotonation of phenol) using tailored laser pulses. This task was accomplished by employing closed-loop AFC optimization of the signal using HD-SFG to monitor the changes in surface chemistry. The deprotonation of the surface bound phenol group was promoted by manipulating vibronic dynamics through two photon excitation with shaped 400nm laser pulses. It is well known that the promotion of the vibrational excitation might lead to more efficient dissociation reaction [43-46]. The control pulse employed in this work contains a significant bandwidth on the order of 2200 cm^{-1} capable of exciting a broad range of motions such as the C-O stretch, at 1230 cm^{-1} and O-H libration at 650 cm^{-1}. Due to the ultrafast nature of excitation and reasonably long vibrational dephasing, multiple excitations of the vibrational modes can come with different relative phase relations, possibly further promoting interesting effects in the deprotonation process. Additional investigation utilizing pump-probe and other techniques are needed to provide a better understanding of such processes. Although the experiments didn't directly reveal the details of the control mechanism, further experiments and modelling for that purpose would be a valuable addition in the future. In the realm of surface control, a fundamental next step would be the demonstration of differential manipulation of competing surface reactions (e.g., either breaking one type of bond vs another or isomerization of one molecule vs another). It would be beneficial to work with species (i.e., containing N-H and O-H bonds) having SFG spectra that can be simultaneously acquired with a given setting of the laser system, covered by the available bandwidth. Such a resolution did not allow us to observe the C-H stretch of phenol at 3090cm^{-1}. The improvement of the spectral resolution will be highly beneficial for a subsequent work as it would allow one to observe the surface spectra in more detail for a better identification

of the processes involved. The time resolved pump-probe experiments will allow one to observe the dynamics of the deprotonation under complex excitation scenarios. In this regard, experiments on a solid support are challenging as they require illumination of fresh portions of the surface for each control pulse. At the same time control of surface molecules on a solid substrate is an important practical goal, as a great number of the technologically important processes can occur in such an environment.

Acknowledgement. A.G. acknowledges support from Army Research Office (grant W911NF-16-1-0014); H.R. acknowledges support from Department of Energy (grant DE-FG02-02ER15344); E.F. and S.B. acknowledge support from National Science Foundation (grant NSF-DMR-1506989) We would like to thank one of the referees for pointing out the recent reference[37].

References

1. R. S. Judson and H. Rabitz, *Physical review letters*, 1992, **68**, 1500.
2. N. Dudovich, D. Oron and Y. Silberberg, *Nature*, 2002, **418**, 512.
3. C. J. Bardeen, V. V. Yakovlev, K. R. Wilson, S. D. Carpenter, P. M. Weber and W. S. Warren, *Chemical Physics Letters*, 1997, **280**, 151-158.
4. R. Levis and H. Rabitz, *The Journal of Physical Chemistry A*, 2002, **106**, 6427-6444.
5. T. Weinacht, J. Ahn and P. H. Bucksbaum, *Nature*, 1999, **397**, 233.
6. A. Goun, D. I. Bondar, O. E. Ali, Z. Quine and H. A. Rabitz, *Scientific reports*, 2016, **6**, 25827.
7. J. L. Herek, W. Wohlleben, R. J. Cogdell, D. Zeidler and M. Motzkus, *Nature*, 2002, **417**, 533.
8. D. J. Pritchard, H. Morgan and J. M. Cooper, *Analytical chemistry*, 1995, **67**, 3605-3607.
9. Y. Liu, Z. Ji, Q. Tang, L. Jiang, H. Li, M. He, W. Hu, D. Zhang, L. Jiang and X. Wang, *Advanced Materials*, 2005, **17**, 2953-2957.
10. S. G. Im, K. W. Bong, B.-S. Kim, S. H. Baxamusa, P. T. Hammond, P. S. Doyle and K. K. Gleason, *Journal of the American Chemical Society*, 2008, **130**, 14424-14425.
11. A. del Campo and E. Arzt, *Chemical reviews*, 2008, **108**, 911-945.
12. D. Meshulach and Y. Silberberg, *Physical Review A*, 1999, **60**, 1287.
13. B. J. Sussman, D. Townsend, M. Y. Ivanov and A. Stolow, *Science*, 2006, **314**, 278-281.
14. P. Král, I. Thanopulos and M. Shapiro, *Reviews of modern physics*, 2007, **79**, 53.
15. A. P. Peirce, M. A. Dahleh and H. Rabitz, *Physical Review A*, 1988, **37**, 4950.
16. A. Zewail, *Advances in Chemical Physics*, 1997, **101**, 3-46.
17. H. Rabitz, *Journal of Modern Optics*, 2004, **51**, 2469-2475.

18. P. Nuernberger, D. Wolpert, H. Weiss and G. Gerber, *Proceedings of the National Academy of Sciences*, 2010, **107**, 10366-10370.
19. P. Nuernberger, D. Wolpert, H. Weiss and G. Gerber, *Physical Chemistry Chemical Physics*, 2012, **14**, 1185-1199.
20. R. Chin, J. Huang, Y. Shen, T. Chuang and H. Seki, *Physical Review B*, 1995, **52**, 5985.
21. R. Chin, J. Huang, Y. Shen, T. Chuang and H. Seki, *Physical Review B*, 1996, **54**, 8243.
22. X. Zhu, H. Suhr and Y. Shen, *Physical Review B*, 1987, **35**, 3047.
23. A. G. Lambert, P. B. Davies and D. J. Neivandt, *Applied Spectroscopy Reviews*, 2005, **40**, 103-145.
24. S. Yamaguchi and T. Tahara, *The Journal of chemical physics*, 2008, **129**, 101102-101102.
25. I. V. Stiopkin, H. D. Jayathilake, A. N. Bordenyuk and A. V. Benderskii, *Journal of the American Chemical Society*, 2008, **130**, 2271-2275.
26. O. P. Vieuxmaire, Z. Lan, A. L. Sobolewski and W. Domcke, *The Journal of chemical physics*, 2008, **129**, 224307.
27. Z. Lan, W. Domcke, V. Vallet, A. L. Sobolewski and S. Mahapatra, *The Journal of chemical physics*, 2005, **122**, 224315.
28. M. Ashfold, B. Cronin, A. Devine, R. Dixon and M. Nix, *Science*, 2006, **312**, 1637-1640.
29. E. Bardez, A. Fedorov, M. N. Berberan-Santos and J. M. Martinho, *The Journal of Physical Chemistry A*, 1999, **103**, 4131-4136.
30. E. L. Hanson, J. Schwartz, B. Nickel, N. Koch and M. F. Danisman, *Journal of the American Chemical Society*, 2003, **125**, 16074-16080.
31. J. Solomon, R. Madix and J. Stöhr, *Surface Science*, 1991, **255**, 12-30.
32. N. Adden, L. J. Gamble, D. G. Castner, A. Hoffmann, G. Gross and H. Menzel, *Langmuir*, 2006, **22**, 8197-8204.
33. J. Serafin and C. Friend, *Surface Science*, 1989, **209**, L163-L175.
34. R. Franke, T. Chasse, P. Streubel and A. Meisel, *Journal of electron spectroscopy and related phenomena*, 1991, **56**, 381-388.
35. R. W. Silverstein, F.; Kiemle, D., in *Spectrometric Identification of Organic Compounds*, USA2005, ch. Characteristic Group Absorptions, p. 124.
36. M. Roth, M. Mehendale, A. Bartelt and H. Rabitz, *Applied Physics B*, 2005, **80**, 441-444.
37. R. Kusaka, S. Nihonyanagi and T. Tahara, *Nature Chemistry*, 2021, **13**, 306-311.
38. S. Nihonyanagi, S. Yamaguchi and T. Tahara, *The Journal of chemical physics*, 2009, **130**, 204704.
39. P. E. Ohno, H. Chang, A. P. Spencer, Y. Liu, M. D. Boamah, H.-f. Wang and F. M. Geiger, *The journal of physical chemistry letters*, 2019, **10**, 2328-2334.
40. D. Spry, A. Goun and M. Fayer, *The Journal of Physical Chemistry A*, 2007, **111**, 230-237.
41. G. Turinici, C. Le Bris and H. Rabitz, *Physical Review E*, 2004, **70**, 016704.
42. O. V. Dorofeeva and O. N. Ryzhova, *The Journal of Physical Chemistry A*, 2016, **120**, 2471-2479.
43. S. Bozpolat, P. Rosenberger, M. F. Ciappina and M. F. Kling, *Physical Review A*, 2019, **100**, 063409.
44. A. Serrano-Jiménez, L. Bañares and A. García-Vela, *Physical Chemistry Chemical Physics*, 2019, **21**, 7885-7893.

45. M. Abe, Y. Ohtsuki, Y. Fujimura, Z. Lan and W. Domcke, *The Journal of chemical physics*, 2006, **124**, 224316.
46. E. Charron, A. Giusti-Suzor and F. H. J. T. J. o. c. p. Meis, 1995, **103**, 7359-7373.